NeuroImage 52 (2010) 224–233

Contents lists available at ScienceDirect

NeuroImage

journal homepage: www.elsevier.com/locate/ynimg

Frequency-dependent neural activity, CBF, and BOLD fMRI to somatosensory stimuli in isoflurane-anesthetized rats

Tae Kim [a,*], Kazuto Masamoto [c,*], Mitsuhiro Fukuda [a], Alberto Vazquez [a], Seong-Gi Kim [a,b]

[a] Department of Radiology, University of Pittsburgh, Pittsburgh, Pennsylvania, USA
[b] Department of Neurobiology, University of Pittsburgh, Pittsburgh, Pennsylvania, USA
[c] Molecular Imaging Center, National Institute of Radiological Sciences, Inage, Chiba, Japan

ARTICLE INFO

Article history:
Received 26 December 2009
Revised 1 March 2010
Accepted 22 March 2010
Available online 27 March 2010

Keywords:
Somatosensory cortex
Isoflurane
Stimulus frequency
fMRI
Laser Doppler flowmetry
Local field potential
BOLD
CBF
Arterial spin labeling
Neural adaptation

ABSTRACT

Inhalation anesthetics (e.g. isoflurane) are preferable for longitudinal fMRI experiments in the same animals. We previously implemented isoflurane anesthesia for rodent forepaw stimulation studies, and optimized the stimulus parameters with short stimuli (1–3-s long stimulation with ten electric pulses). These parameters, however, may not be applicable for long periods of stimulation because repetitive stimuli induce neural adaptation. Here we evaluated frequency-dependent responses (pulse width of 1.0 ms and current of 1.5 mA) for 30-s long stimulation under 1.3–1.5% isoflurane anesthesia. The cerebral blood flow (CBF) response (using laser Doppler flowmetry: CBF_{LDF}) and field potential (FP) changes were simultaneously measured for nine stimulus frequencies (1–24 Hz). CBF (using arterial spin labeling: CBF_{ASL}) and blood oxygenation level dependent (BOLD) fMRI responses were measured at 9.4 T for four stimulus frequencies (1.5–12 Hz). Higher stimulus frequencies (12–24 Hz) produced a larger FP per unit time initially, but decreased more rapidly later due to neural adaptation effects. On the other hand, lower stimulus frequencies (1–3 Hz) induced smaller, but sustained FP activities over the entire stimulus period. Similar frequency-dependencies were observed in CBF_{LDF}, CBF_{ASL} and BOLD responses. A linear relationship between FP and CBF_{LDF} was observed for all stimulus frequencies. Stimulation frequency for the maximal cumulative neural and hemodynamic changes is dependent on stimulus duration; 8–12 Hz for short stimulus durations (<10 s) and 6–8 Hz for 30-s stimulation. Our findings suggest that neural adaptation should be considered in determining the somatosensory stimulation frequency and duration under isoflurane anesthesia.

Introduction

Functional magnetic resonance imaging (fMRI) during electrical stimulation of the rodent forepaw has been used to investigate the biophysical properties of fMRI signals (Kida et al., 2001; Lee et al., 1999; Mandeville et al., 1998; Silva and Kim, 1999) because of its well-characterized neural activity, abundant fMRI data and large fMRI signal change. Anesthesia is necessary for fMRI in animal models to minimize motion and stress of the animals during the experiments. Most rodent fMRI studies have been performed with α-chloralose anesthesia (Bock et al., 1998; Kida et al., 2001; Lee et al., 1999; Mandeville et al., 1998; Silva and Kim, 1999). However, α-chloralose-anesthetized animals have to be euthanized after the experiment, which hampers its use for survival experiments (Silverman and Muir, 1993).

Inhalation anesthetics (e.g., isoflurane) are preferable for longitudinal fMRI experiments such as tracking the same subjects during the development of brain functions (Colonnese et al., 2008) and functional recovery after brain injury (Dijkhuizen et al., 2001; Dijkhuizen et al., 2003; Schmitz et al., 1998). Different anesthetics likely alter the properties of the neural activity and the neurovascular coupling mechanism because they act on different receptors (Alkire et al., 2008). For instance, the maximal response to forepaw electrical stimulation under α-chloralose anesthesia was observed in the condition of stimulus frequencies between 1 and 3 Hz, stimulus amplitude of 0.5 to 2 mA and width of 0.3 ms during stimulus durations of 30 to 45 s (Brinker et al., 1999; Gyngell et al., 1996; Huttunen et al., 2008; Keilholz et al., 2004; Sanganahalli et al., 2008; Silva et al., 1999). With isoflurane anesthesia, the maximal responses to forepaw stimulation were induced by a stimulus frequency of 12 Hz, current of at least 1.4 mA and pulse width of at least 1.0 ms for fixed 10-pulse stimulus trains (Masamoto et al., 2007). Further, for enflurane anesthesia, a stimulus frequency of 10 Hz was optimal for 2-s long simulation (Sheth et al., 2004). These results suggest that the

* Corresponding authors. Kim is to be contacted at the Department of Radiology, University of Pittsburgh, 3025 East Carson Street, Pittsburgh, PA 15203, USA. Fax: +1 412 383 6799. Masamoto, Center for Frontier Science and Engineering, The University of Electro-communications, 1-5-1 Chofugaoka, Chofu, Tokyo 182-8585, Japan. Fax: +81 42 443 5930.
E-mail addresses: tak19@pitt.edu (T. Kim), masamoto@mce.uec.ac.jp (K. Masamoto).

1053-8119/$ – see front matter © 2010 Elsevier Inc. All rights reserved.
doi:10.1016/j.neuroimage.2010.03.064

neurovascular coupling properties characterized in one anesthetic should not be applied to other anesthetics. Thus, optimal stimulation parameters should be determined by maximizing the evoked neural activities under each anesthetic condition (Brinker et al., 1999; Gyngell et al., 1996; Huttunen et al., 2008; Keilholz et al., 2004; Masamoto et al., 2007; Sanganahalli et al., 2008).

Repetitive somatosensory stimuli are known to cause neural adaptation. The degree of adaptation is dependent on the stimulus frequency and duration (Chung et al., 2002; Khatri et al., 2004), and probably the type of anesthetic used. Low frequency stimuli (e.g., 1 Hz) evoke similar magnitude of neural activities over time, but increasing the stimulus frequency (i.e. shortening an inter-pulse interval) induces a more rapid and pronounced adaptation in neural activity over time in the cortex. Therefore, our previous stimulus frequency of 12 Hz optimized with a short stimulus duration (less than 1 s with fixed 10-pulse) under isoflurane anesthesia may not induce largest neural activity and hemodynamic response for longer stimulus duration, which is preferable for many fMRI studies. Thus, in order to maximize the evoked hemodynamic fMRI response for long stimulus duration under isoflurane anesthesia, it is crucial to determine the detailed stimulus frequency- and duration-dependent relationships between neural activity and hemodynamic responses.

In this work, we measured local field potential (FP), cerebral blood flow (CBF) and blood oxygenation level dependent (BOLD) fMRI responses in the rat somatosensory cortex during 30-s forepaw stimulation at various frequencies under 1.3–1.5% isoflurane anesthesia. Two separate animal groups were used: one with simultaneous measurements of FP and CBF using laser Doppler flowmetry (CBF_{LDF}), and another with concurrent recordings of CBF using arterial spin labeling (ASL) (CBF_{ASL}) and BOLD fMRI at 9.4 T. Neural activities were determined as a function of the stimulus frequency and the temporal and spatial characteristics of fMRI responses at different stimulus frequencies were also assessed. In order to investigate the dynamic signal changes for different stimulus frequencies, neural activities and hemodynamic responses were divided into three 10-s stimulus periods over the stimulus duration (e.g., 0 to 10, 10 to 20, and 20 to 30 s from stimulus onset).

Methods

Animal preparation

The animal protocol was approved by the University of Pittsburgh Animal Care and Use Committee. Twelve male Sprague–Dawley rats weighing 350–450 g (Charles River Laboratories, Wilmington, MA) were studied; FP and CBF_{LDF} data were measured in six animals, while BOLD and CBF_{ASL} were obtained from a separate group of six animals scanned in a 9.4 Tesla MRI scanner. The animals were initially induced with 5% isoflurane and intubated. Then, the isoflurane level was reduced to 2% for surgery; the femoral artery and vein were catheterized to monitor arterial blood pressure and to administrate supplemental fluid, respectively. Arterial blood pressure was continuously recorded with polygraph data acquisition software (ACK100W AcqKnowledge Software, BIOPAC systems, Inc., Goleta, CA). Then, the isoflurane level was reduced to 1.3–1.5% in air supplemented with O_2 to attain a total O_2 level of about 30% throughout recording. It is noted that nitrous oxide (N_2O) was not used because apparent neural and hemodynamic responses to forepaw stimulation were not observed when the mixture of both N_2O and isoflurane was used. To ensure maintaining a normal arterial oxygen saturation level under anesthetized conditions, an inhalation oxygen level with slightly higher than air (21%) was used. Arterial blood gases were periodically measured throughout the experiment with a blood gas analyzer (Stat profile pHOx, Nova Biomedical, MA) and the ventilation rate and volume were adjusted to maintain normal physiological conditions. Rectal temperature was maintained at 37.5 ± 0.5 °C with a feedback-controlled heating pad.

Forepaw stimulation

Electrical stimulus pulses (1.0 ms pulse width and ~1.5 mA current) were generated using a pulse generator (Master 8, A.M.P.I., Israel) and delivered using a constant current isolator (Iso-Flex, A.M.P.I., Israel) to one forepaw using two needle-electrodes inserted under the palmar skin between digits two and four. Each stimulus run consisted of a 30-s pre-stimulus baseline, 30-s stimulus period, and 50-s post-stimulus period. The inter-stimulus period was greater than 3 min. The stimulus frequency was varied over different runs in a randomized order; nine frequencies (1, 1.5, 3, 4, 6, 8, 12, 16 and 24 Hz) were examined for the FP and LDF measurements, while four frequencies (1.5, 3, 6 and 12 Hz) were chosen for the fMRI studies, based on preliminary FP and CBF_{LDF} data due to the consideration of experimental time.

Conventional physiology studies conducted outside the magnet

FP activity and CBF responses were concurrently recorded with a microelectrode and LDF, as described previously (Masamoto et al., 2007). Briefly, a 5 mm × 7 mm portion of the left skull, centered 3.5-mm lateral and 0.5-mm rostral from bregma, was thinned with a drill. The thinned area was then immersed in oil for transparency. The activation focus area in response to stimulation (6 Hz in frequency and 4 s in duration) was mapped using optical imaging of intrinsic signals over the primary somatosensory cortex (band pass = 620 ± 10 nm). Then, a tungsten microelectrode (<1 MΩ, World Precision Instruments, Inc., Sarasota, FL) was inserted to a depth of 0.5 mm perpendicular to the cortical surface at the center of activation focus area and a reference electrode was placed on the scalp. A needle-type LDF probe (PeriFlux 4001 Master system, Perimed, Sweden) was placed on the thinned skull preparation within 0.5 mm of the location of the FP recording electrode while avoiding large visible pial vascular areas. The FP signal was measured using the Neural Data Acquisition software (Plexon, Inc., Dallas, TX) with a sampling rate of 5 kHz, and the LDF signal was recorded by BIOPAC data acquisition software (ACK100W AcqKnowledge Software, BIOPAC systems, Inc., Goleta, CA) with a sampling rate of 100 Hz.

All runs from identical stimulus frequency conditions were averaged for each animal. The FP amplitude induced by each stimulus pulse was obtained by measuring the peak intensity, i.e., minimum to maximum observed over the period of 5 to 20 ms after each pulse. All FP amplitudes in each animal were first normalized by the average of the first FP amplitude across all the stimulus frequencies. Since the number of stimulus pulses is different for different frequencies (for example, the number of stimulus in 12 Hz is eight times more than that of 1.5 Hz at a given period), bin-FP was calculated by summation of FP over 2 s, reflecting a net FP activity per unit 2-s time, and was used to compare FP time courses for different frequency stimuli. Summation of bin-FP values (ΣFP) over 10 s were also calculated from 0 to 10 s, 10 to 20 s, and 20 to 30 s from stimulation onset. This metric was used to compare FP trends for different frequency stimuli. LDF data were averaged every 0.2 s and normalized by the average signal intensity of the pre-stimulus period for each stimulus frequency in each animal. The integral of the CBF_{LDF} changes (ΣCBF_{LDF}) over non-overlapping 10-s periods were also determined from the area under the CBF_{LDF} curve during the stimulus periods (i.e., 0–10 s, 10–20 s and 20–30 s from stimulus onset). To directly compare FP with CBF_{LDF}, cumulated FP and cumulative CBF_{LDF} values were calculated as sums of data from stimulation onset time (0) during 30-s stimulation period, and plotted against each other for each stimulus frequency.

Functional MRI studies

ASL studies were performed to obtain CBF_{ASL} and BOLD fMRI responses, as described previously (Kim et al., 2007). Briefly, all MRI measurements were performed on a 9.4 T magnet with a bore size of 31 cm in diameter, interfaced to a Unity INOVA console (Varian, Palo Alto, CA). Two actively-detunable radio frequency (RF) coils were used: a surface coil (2.3 cm in diameter) was positioned on top of the head for image acquisition, and a butterfly-shaped surface coil was positioned in the neck region for ASL. All coronal images were acquired using a single-shot gradient-echo (GE) echo planar imaging (EPI) technique with a slice thickness = 2 mm, matrix size = 64 (readout) × 32 (phase-encode) and field of view = 2.56 × 1.28 cm^2. The repetition time (TR) was 2.5 s consisting of 2.4-s spin-preparation period and 0.1-s imaging time, and the echo time (TE) was 20 ms. In three animals, a bipolar gradient pair ($b = 30$ s/mm^2) was applied after the excitation pulse to suppress signal contributions from large arterial vessels. Twenty-two pairs of arterial spin labeled (*lab*) and unlabeled (*unlab*) images were acquired; 6 pairs during pre-stimulus baseline, 6 pairs during stimulation and 10 pairs during the post-stimulus period. The acquisition order of *lab* and *unlab* images was alternated between experimental runs; the image order in run *A* was $unlab_{A1}$, lab_{A1}, $unlab_{A2}$, ⋯, lab_{A22}, while in run *B* it was lab_{B1}, $unlab_{B1}$, lab_{B2}, ⋯, $unlab_{B22}$, where subscripts refer to both the run and the pair. Each fMRI run was repeated 10–15 times for each stimulus frequency.

In each animal, all runs from identical stimulus conditions were averaged. To obtain CBF-weighted images from run *A* and *B*, pair-wise subtracted images were calculated such as $\Delta S_{A1} = unlab_{A1} - lab_{A1}$ and $\Delta S_{B1} = unlab_{B1} - lab_{B1}$. Then, time-matched subtracted images in run *A* and *B* (ΔS) were averaged to obtain a single time series. Similarly, unlabeled control images in both runs (S_{unlab}) were combined such as $(unlab_{A1} + unlab_{B1})/2$ to match time points of ΔS series. Time series with 43 data points were generated from both runs of *A* and *B*. Using ΔS and S_{unlab} series, CBF (in units of ml/g/min) was calculated at every time point on a pixel-by-pixel basis using

$$CBF = \frac{\lambda}{T_1} \cdot \left(\frac{\Delta S}{2 \cdot \alpha \cdot S_{unlab} \cdot \zeta - \Delta S} \right) \quad (1)$$

where λ is the tissue–blood partition coefficient of 0.9 ml/g (Herscovitch and Raichle, 1985); T_1 is the T_1 value of tissue without flow contribution, which is 2.0 s (Kim and Kim, 2005); α is the labeling efficiency of arterial spins, $\alpha = \alpha_0 \cdot \exp(-\tau / T_{1a})$, where the labeling efficiency at labeling plane (α_0) = 0.7, the longitudinal relaxation time of arterial blood (T_{1a}) = 2.3 s, and the transit time of labeled spins (τ) = 0.3 s without the bipolar gradient and 0.6 s with the bipolar gradient. The correction term (ζ) in Eq. (1) corrects for insufficient relaxation due to relatively short TR, because labeled and unlabeled images were acquired in an interleaved manner and the spin-labeling time was much less than 3 times T_1^* (Barbier et al., 1999); $\zeta = [1 - \exp(-(t_{lab} - \tau)/T_1^*)]$, where t_{lab} is the time span for spin-preparation period (2.4 s); and T_1^* is the apparent T_1 value of tissue including CBF contributions, which is ~1.9 s (Kim and Kim, 2002).

For each frequency in each animal, unlabeled (control) and pair-wise subtracted (ΔS) images were used to obtain BOLD and CBF_{ASL} responses induced by forepaw stimulation, respectively. Two analyses were performed; average time courses were obtained and fMRI maps were generated. (i) Since a rat brain atlas (Paxinos and Watson, 1986) shows the forelimb somatosensory cortical area in a hemisphere to be about 1.5 × 1.5 mm^2 in the coronal plane (0.2 and 0.3 mm anterior to bregma), a 16-pixel ROI (1.6 × 1.6 mm^2) centered over this anatomically-defined area on the side contralateral to stimulation was used in each animal. For ROI analysis, all pixels within the ROI were averaged, regardless of whether pixels were active. Full width at half maximum (FWHM), time-to-peak (TTP) and peak amplitude were measured from the response curves to investigate temporal characteristics of the hemodynamic changes. The integral of BOLD (ΣBOLD) and CBF_{ASL} changes (ΣCBF_{ASL}) were calculated from the area under the response curve over stimulus periods of 0–10 s, 10–20 s and 20–30 s from stimulus onset. (ii) To investigate stimulus duration-dependent fMRI responses, three *t*-maps were generated with a threshold of $t \geq 3.0$ by comparing baseline data with images acquired during three divided stimulus periods of 0–10 s, 10–20 s and 20–30 s from stimulation onset. For these *t*-maps, the first point of data after stimulation onset was excluded due to delayed hemodynamic responses. The baseline condition included all pre-stimulus and post-stimulus images following 6 s after stimulation offset. A general linear model (GLM) analysis was also performed on the data to assess the spatial extent of the responses considering the full duration of the responses. To capture the temporal changes over different frequencies, the average data over the 16-pixel ROI (over all animals) was used to fit a representative gamma function for each frequency using Matlab (Mathworks, Inc., Natick, MA). The gamma functions were then used as reference in the GLM analysis and the correlation coefficients were calculated for each frequency in each animal. Then, *t*-values were calculated and functional activation maps were generated using a threshold of $t \geq 3.0$. The number of active pixels within the contralateral cortex was determined. Individual results were averaged and group data are reported as mean ± SD. Statistical analyses were performed using a repeated measure ANOVA and a post hoc analysis for the criterion of statistical significance (SPSS, SPSS Inc, Chicago, IL).

Results

Physiological parameters for baseline condition

No significant differences in the baseline conditions were observed between the two separate animal groups: pH = 7.47 ± 0.01, $PaCO_2$ = 35.9 ± 1.5 mm Hg, PaO_2 = 142 ± 10 mm Hg, and mean arterial blood pressure (MABP) = 89 ± 10 mm Hg for the FP and LDF studies (n = 6 animals); pH = 7.47 ± 0.02, $PaCO_2$ = 38.2 ± 3.7 mm Hg, PaO_2 = 132 ± 20 mm Hg, and MABP = 93 ± 10 mm Hg for the fMRI studies (n = 6 animals). In addition, no significant changes in arterial blood pressure were observed during somatosensory stimulation.

Conventional physiology (FP and LDF) measurements

The averaged temporal profiles of FP amplitude and CBF_{LDF} responses induced by the stimulus frequencies which were used in the fMRI studies (1.5, 3, 6, and 12 Hz) are presented in Fig. 1. An increase in the stimulus frequency produced a pronounced reduction in FP amplitudes over time (Fig. 1A). The magnitude of neural activity reached a pseudo-steady state within one second after stimulation onset (see the inset plot in Fig. 1A for initial 2-s data points), and then continued to decrease slowly over time. Since the number of stimulus pulses is different for different frequencies over a given period, bin-FP time courses calculated by the summation of FPs over 2-s bins (Fig. 1B) to compare FP activities across the different frequencies. The bin-FP amplitude was largest for the 12 Hz stimulus frequency over the first 2 s from stimulus onset. The bin-FP amplitude for the higher stimulus frequencies (6 and 12 Hz) decreased more rapidly over time, while the bin-FP amplitude for lower frequency stimuli (1.5 and 3 Hz) was similarly maintained over the entire stimulation period. The CBF_{LDF} time courses were similar to the bin-FP time courses (Fig. 1C); the largest CBF_{LDF} responses (~70% peak amplitude) were observed for the 6 and 12 Hz stimulus frequencies, but the responses decreased over the stimulation period, while the CBF_{LDF} for the 1.5 and 3 Hz stimulation remained relatively constant over the stimulus period.

To compare the frequency-dependence in the FP and CBF responses over different stimulus periods, the ΣFP and ΣCBF_{LDF} over

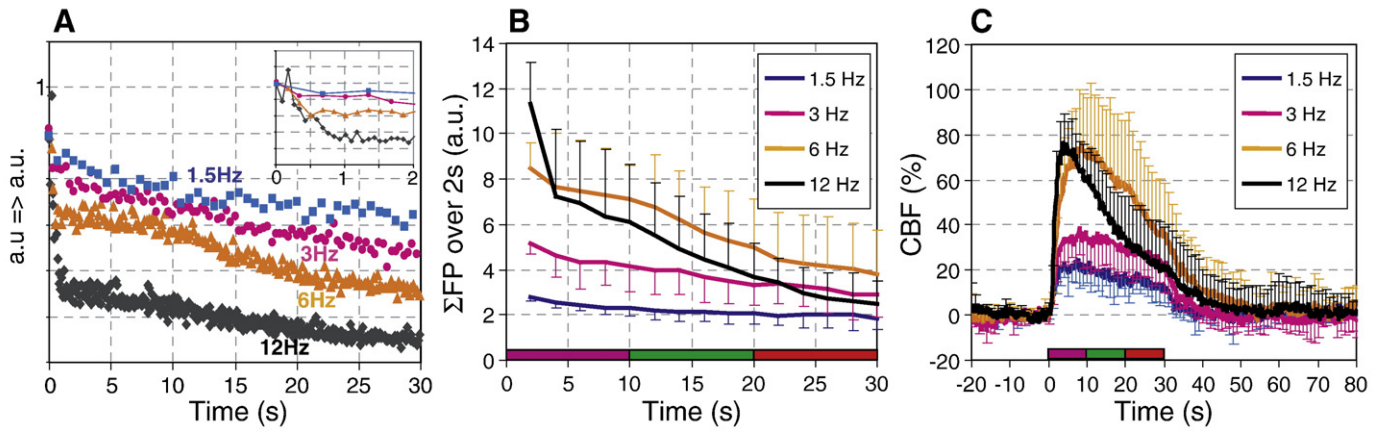

Fig. 1. Averaged temporal profiles of evoked FP and CBF_{LDF} responses ($n=6$ animals). (A) FP amplitude time courses for four stimulus frequencies which were used in the fMRI studies. Each data point indicates the mean of the 6 animal studies for each individual stimulus pulse. The inserted plot shows the initial 2 s of data; the neural activity reached a pseudo-steady state within one second after simulation onset. (B) Bin-FP per 2-s unit time was calculated to take into account of the different numbers of stimulus pulses over a given period. The bin-FP amplitude for higher frequency stimuli was initially larger, but decreased more quickly over time, while the bin-FP amplitude for lower frequency stimuli was relatively maintained over the entire period of stimulation. (C) Frequency-dependent CBF responses measured by LDF. Similar trends as FP responses were observed. Three color bars underneath time courses indicate the time periods for determining ΣFP and ΣCBF in Fig. 2. Error bar: SD every 2 s.

0–10 s, 10–20 s, and 20–30 s after stimulation onset were plotted as a function of stimulus frequency (Figs. 2A and B). For the first 10-s stimulus period, stimulus frequencies ≥6 Hz induced similar ΣFP responses that are also larger than data with frequencies <4 Hz (open square symbols in Fig. 2A). For 10–20-s stimulus period, the highest response was observed at a stimulus frequency of 8 Hz (open triangles for 10–20 s). For the last 10-s stimulus period, FP responses to the 4–8 Hz stimulus frequencies were significantly larger than those of 12 Hz (open circles for 20–30 s). These temporal characteristics of ΣFP response resulted in the highest summed response to 30-s long

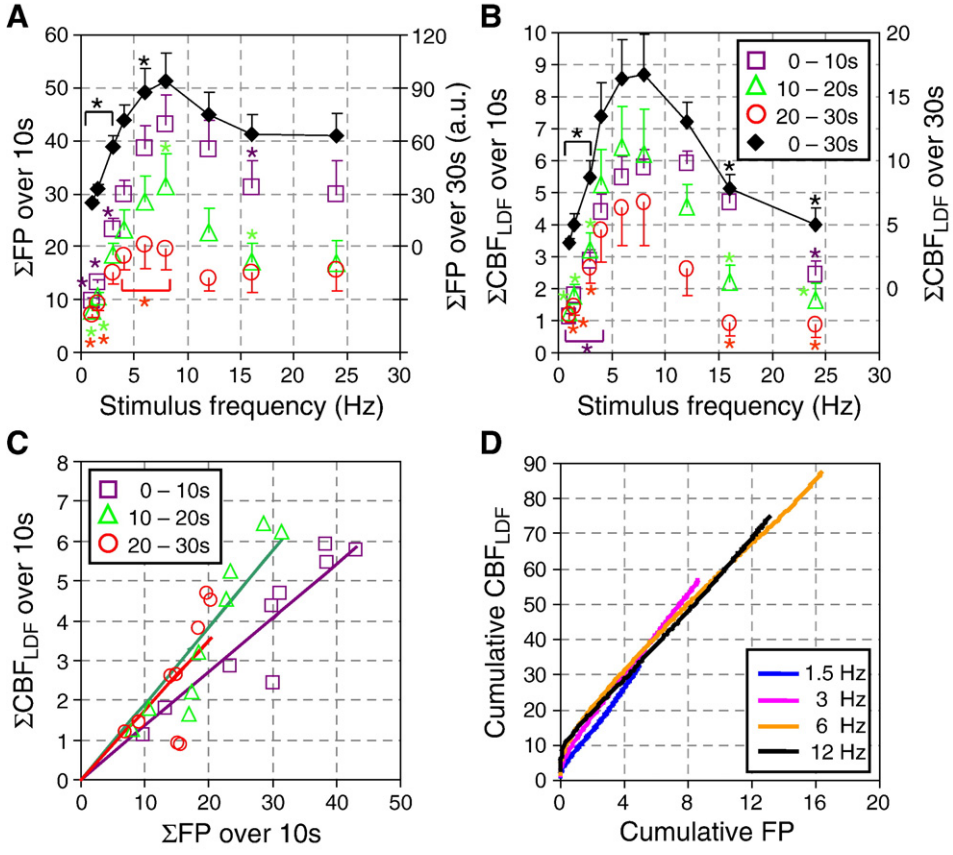

Fig. 2. Summation of FP change (A) and the area under CBF_{LDF} curve (B) over 10 s (left axis) and 30 s (right axis) as a function of stimulus frequency ($n=6$ animals). To examine frequency-dependence in the FP and CBF responses over different stimulus periods, signal changes were compared over three stimulus periods of 0–10 s (open squares), 10–20 s (open triangles) and 20–30 s (open circles). Data for 0–30 s are summation of these three stimulation periods (closed diamonds). Statistically significant differences between the responses at 12 Hz vs. other frequencies were obtained ($^{*}p<0.05$). Error bars: SEM. (C) ΣFP and ΣCBF changes over 10-s periods were compared. (D) The relationship between the cumulative FP and the cumulative integral of the CBF_{LDF} response for all stimulation frequencies are shown (mean R of four frequencies = 0.998). These high correlations indicate that the hemodynamic responses are highly coupled with the neural responses. The neurovascular relationship is independent of stimulation frequencies and durations.

stimulation with 6–8 Hz stimulus frequency (closed diamond symbols in Fig. 2A). Similar trends of frequency-dependent CBF_{LDF} responses were observed (Fig. 2B). For the first 10-s stimulation period, the large ΣCBF_{LDF} responses were detected for a broad range of stimulus frequencies (4–16 Hz), while the highest CBF_{LDF} responses were observed for 6–8 Hz when later stimulus periods were considered.

The coupling between neural and vascular response on stimulation frequencies and durations was investigated. ΣFP and ΣCBF_{LDF} changes over 10-s periods were compared (Fig. 2C). A linear relationship between FP and CBF_{LDF} was observed, independent of stimulus duration. The cumulative changes in the neural and hemodynamic responses during 30-s stimulation are also plotted for the different stimulus frequencies (Fig. 2D). The cumulative FP and cumulative CBF_{LDF} were highly correlated for all the different stimulation frequencies (mean R of four frequencies = 0.998). A similar linear relationship was observed between FP and CBF changes, independent of the stimulus frequency.

BOLD and CBF fMRI measurements

The averaged BOLD and CBF_{ASL} fMRI time courses measured from the 16-pixel ROI over the contralateral somatosensory area are shown in Fig. 3 ($n = 6$). Both BOLD and CBF_{ASL} time courses behave similar frequency-dependent trends (Figs. 3A vs. B), and resemble CBF_{LDF} and bin-FP time courses (Figs. 1B and C). Higher stimulus frequencies induced a higher peak amplitude, but also a larger reduction of both BOLD and CBF_{ASL} responses over the stimulus duration due to neural adaptation. The peak amplitude was increased with stimulus frequency (Fig. 3D), whereas FWHM and TTP were decreased with stimulus frequency (Fig. 3C). As a result, the fMRI maps and signal changes are closely dependent on the stimulus period. In order to evaluate the effect of stimulus period on the fMRI responses, we generated statistical maps from the fMRI data over three different stimulus periods (see color bars underneath time courses in Fig. 3).

Results of the stimulus period-dependent fMRI maps are presented in Fig. 4. BOLD fMRI maps are overlaid on T_1-weighted images (Fig. 4A), and the CBF_{ASL} fMRI maps are overlaid on quantified baseline CBF_{ASL} maps in units of ml/g/min (Fig. 4B) from one animal. In all frequency studies, localized activation was observed in the contralateral somatosensory cortex. Statistical values and the number of statistical significant pixels were dependent on the stimulus frequency and period. In general, both statistical values and the number of active pixels are the highest for the maps obtained from the first 10-s data in all frequencies, and decrease larger for higher frequency over time. Especially, only a few or no active pixels were detected for 20–30-s data from 12 Hz stimulus frequency. Trends showing a less number of active pixels for the later stimulus periods are also reflected in the average BOLD and CBF_{ASL} time courses (Figs. 3A and B). To quantify these observations, the number of activated pixels was determined for the BOLD (Fig. 4C) and CBF_{ASL} studies (Fig. 4D). Interestingly, for the first 10 s of stimulation, the number of activated pixels was not statistically different ($p > 0.05$, repeated ANOVA test) across the different stimulus frequencies, even if the magnitudes (percentage changes) of the fMRI responses from higher frequencies were larger. For the later stimulus periods (10–20 s and 20–30 s), the number of active pixels was significantly decreased for the 12 Hz stimulus frequency, while it was less affected for the lower frequencies (Figs. 4C and D). However, the GLM analysis performed using fitted gamma functions for each stimulus frequency

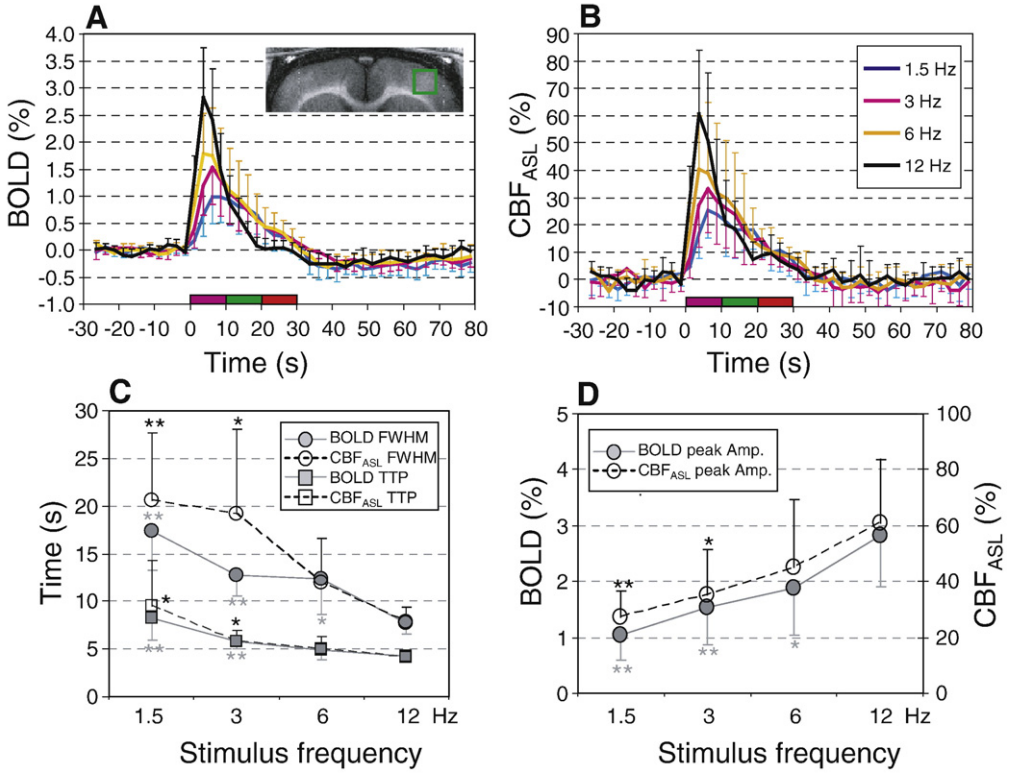

Fig. 3. The averaged BOLD (A) and CBF_{ASL} fMRI (B) time courses ($n = 6$ animals) for four different frequencies, obtained from the 16-pixel contralateral somatosensory cortex ROI. The green box in the inserted image shows the ROI (A). The BOLD and CBF_{ASL} responses were highly correlated in all frequencies ($R > 0.95$). The largest peak response was detected at 12 Hz stimulus frequency but this elevated response was quickly declined. However, at lower frequencies, the elevated signals were maintained during the entire stimulation period. The three color bars underneath the time courses indicate the time periods for the generation of functional maps shown in Fig. 4. FWHM and TTP (C), and peak amplitude (D) of time courses were measured. FWHM and TTP were decreased with stimulus frequency, while peak amplitude was increased with stimulus frequency. Statistically significant differences between the responses at 12 Hz vs. other frequencies were obtained ($^{*}p < 0.05$, $^{**}p < 0.01$). Error bars: SD.

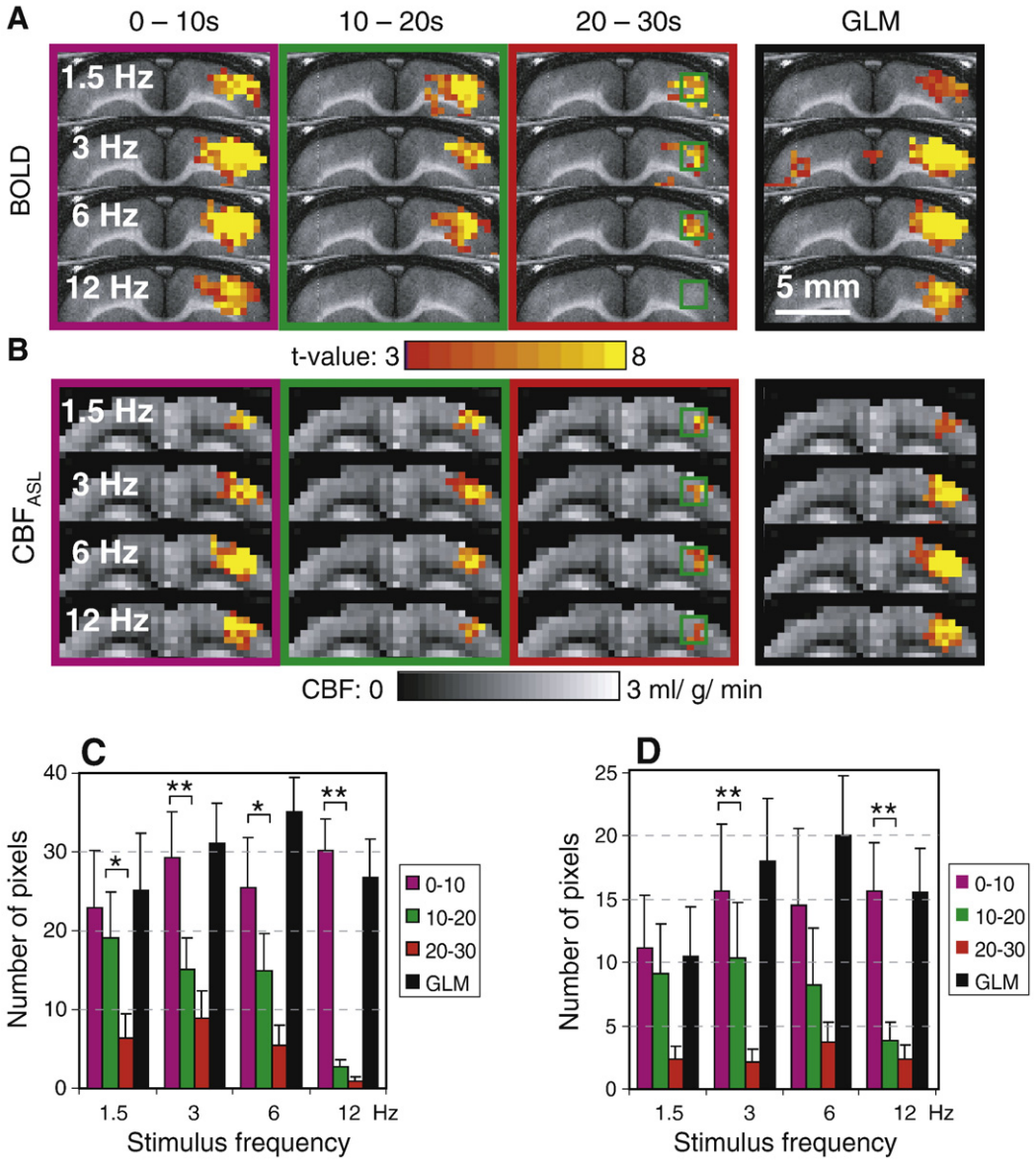

Fig. 4. Frequency-dependent fMRI results. fMRI *t*-value maps were generated from images acquired during baseline vs. three stimulus periods for the different frequencies. BOLD fMRI maps (A) were overlaid on T_1-weighted images, while CBF_{ASL} fMRI maps (B) were overlaid on quantified baseline CBF maps in units of ml/g/min from one animal (grayscale bar indicates quantified CBF value). The 30-s stimulation data were divided into three stimulus periods: 0–10 s, 10–20 s, and 20–30 s after stimulation onset. In addition, the GLM analysis was performed with a gamma function obtained for each frequency. Each color of box represents the stimulus period bar shown in Fig. 3. The number of activated pixels with a *t*-value ≥ 3 in the contralateral hemisphere was determined. The average number of activated pixels (n=6 animals) is plotted for BOLD (C) and CBF_{ASL} (D). The area of activation decreased with later stimulus periods at 12 Hz frequency, while it was relatively maintained over entire stimulus periods at lower stimulus frequencies. However, fMRI maps from the GLM analysis (black color boxes in panels A and B) yield a similar number of activated pixels (black color bars in panels C and D) over different stimulus frequencies. Statistical comparisons were performed between the 0–10 s and 10–20 s stimulus period, between 10–20-s and 20–30-s stimulus period, and between GLM data across each stimulus frequency (paired student *t*-test, $^{*}p<0.05$, $^{**}p<0.01$). Color-scale bars: *t*-value; error bars: SEM.

showed that the overall statistical maps and the numbers of activation pixels were similar over all stimulus frequencies (black boxes and bars in Fig. 4).

The ΣBOLD and ΣCBF_{ASL} fMRI responses are plotted as a function of stimulus frequencies for different stimulus periods (Figs. 5A and B). The highest ΣBOLD and ΣCBF_{ASL} responses were observed at the 12 Hz stimulus frequency for the first 10-s period (open square symbols), but less signal changes for the later stimulus periods (open triangles and open circles symbols). At the lower frequencies, ΣBOLD and ΣCBF_{ASL} responses were larger than those at 12 Hz in the later period of stimulation (open triangles and open circles symbols). Overall the highest responses were observed at 6 Hz for the 30-s long stimulus duration albeit statistically insignificant (closed diamond symbols). This indicates that the stimulation duration is important for determining the optimal stimulus frequency. BOLD and CBF_{ASL} fMRI responses were also highly correlated in all the frequencies, indicating their tight coupling (Figs. 5C and D, $R>0.95$).

Discussion

We have demonstrated that the temporal characteristics of hemodynamic response depend on the stimulus duration and frequency in the isoflurane-anesthetized rat forepaw model. The hemodynamic response was largest at the stimulus frequency of 8–12 Hz during the early period for 30-s long stimulus duration, whereas the responses were largest at stimulus frequencies of 6–8 Hz over the later stimulus periods. If the

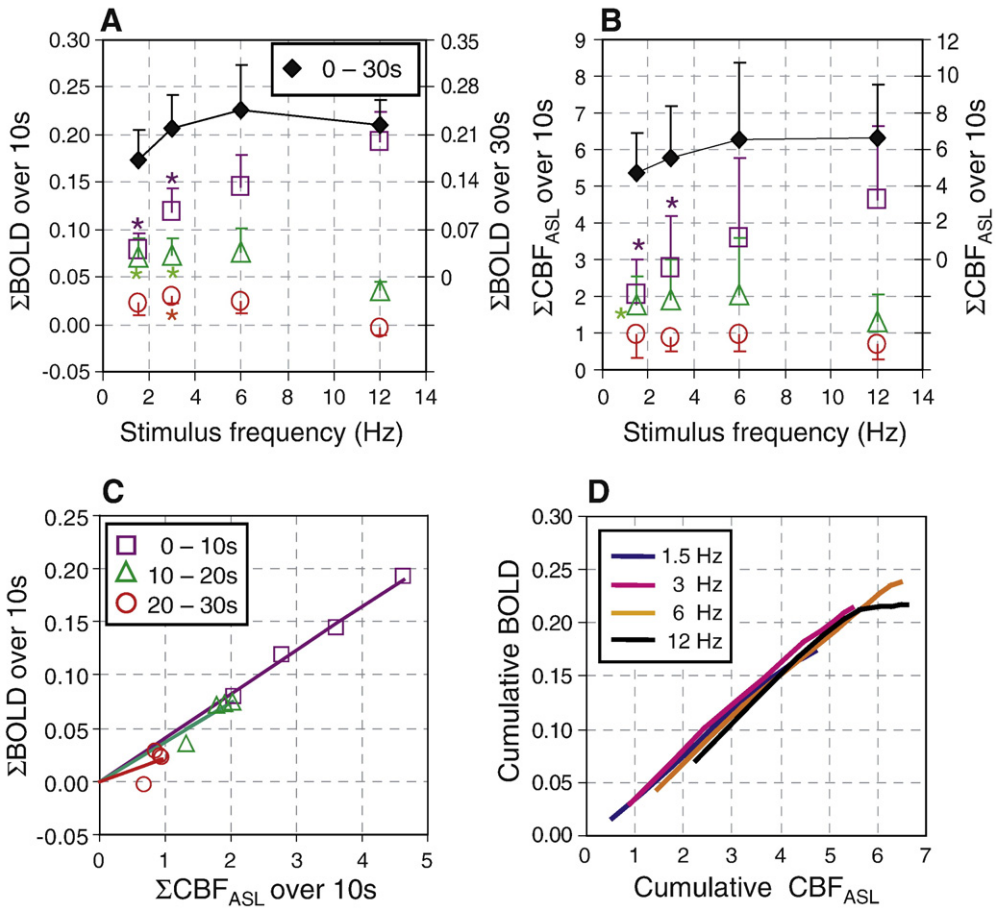

Fig. 5. The area under the BOLD (A) and CBF_{ASL} (B) signal changes is plotted as a function of stimulus frequency. The signal changes were calculated over three stimulus periods (scales at left axis) of 0–10 s (open squares), 10–20 s (open triangles) and 20–30 s (open circles). Closed black diamond symbols (scales at right axis) present the summation of three stimulus durations (0–30 s). The largest signal changes appeared to be 12 Hz for 0–10-s stimulus period, but significantly decreased for the later stimulus period. Statistical differences between the responses at 12 Hz vs. other frequencies were obtained ($^{*}p<0.05$). Error bars: SD ($N=6$ animals). (C) ΣCBF_{ASL} and ΣBOLD changes over 10-s periods were compared. (D) Cumulative responses of BOLD and CBF_{ASL} were highly correlated in each stimulus frequency, showing their tight coupling.

stimulus duration is longer than 30 s, the stimulus frequency for maximal integrated hemodynamic responses may be even lower than 6–8 Hz. This frequency-dependence of the hemodynamic responses on stimulus duration was consistent with that of measured neural activity, showing a linear coupling between neural activity and hemodynamic responses (Fig. 2C). Neural activity was initially larger for high stimulus frequency, but neural adaptation to the high stimulus frequency made the FP responses smaller than low frequency for later stimulus periods (Figs. 1B and 2A). Unlike isoflurane, the dependence of the optimal stimulus frequency on stimulus duration was not found under α-chloralose-anesthetized rats (Kida and Yamamoto, 2008; Ureshi et al., 2004). This is because the optimal stimulus frequency for α-chloralose anesthesia was found to be 1–3 Hz and the reduction of cortical neural activity due to the neural adaptation is small at these low frequencies. Cortical neurons become more adapted to highly repeating strong stimuli where their activity rapidly decreases over the stimulus period. However, this sensory adaptation may not be apparent in human and behaving animals. During behaviorally activated states, sensory responses are already adapted because of continuous sensory inputs and thus further adaptation to stimulation is suppressed, while sensory adaptation has been clearly observed in quiescent states such as anesthesia, slow-wave sleep, and awake immobility (Castro-Alamancos, 2004).

The mechanism of neural adaptation is not understood well. High temporal frequency stimulation quickly decreases cortical neural responses over the stimulus presentation period. Why do cortical neurons fail to respond to high temporal frequency stimulation? Since adaptation is more pronounced in the cortex compared to the thalamus, local cortical mechanisms are mainly involved in adaptation. Krukowski and Miller proposed a model to explain a cortical low-pass temporal frequency tuning. In their circuit model, NMDA-mediated slow thalamocortical inputs are crucial, in addition to thalamocortical inhibition (Krukowski and Miller, 2001). Chung et al. found that the depression of thalamocortical synapses causes a rapid response decline in the rat barrel cortex (Chung et al., 2002). However, this reduction of synaptic input to the postsynaptic cell has not been universally found. For instance, this mechanism is not likely responsible for neural adaptation in the cat visual cortex. Carandini and Ferster reported that neural adaptation resulted in a tonic hyperpolarization without changing synaptic input (Carandini and Ferster, 1997). This tonic hyperpolarization is not caused by an increase in tonic inhibition, but by a decrease in tonic excitation. In fact, blocking $GABA_A$-mediated inhibitory neurons has little effect on adaptation (DeBruyn and Bonds, 1986; McLean and Palmer, 1996; Vidyasagar, 1990). It has not been clear, however, how the tonic excitation is decreased. Petersen suggests a short-term depression of synapses in recurrent connections between excitatory layer 4 neurons (Petersen, 2002). Slow kinetic receptors such as NMDA, metabotropic and $GABA_B$ might be involved in this process (for review, see Kohn, 2007). These receptors are activated late and remain active for a few hundred milliseconds, which appear to match adaptation time courses. Further investigations for cellular mechanisms of adaptation are necessary to understand the neural response property.

The degree of adaptation during stimulus presentation also depends on anesthetic types and probably on the depth of anesthesia. The molecular targets of anesthetics have been explored and at least three targets have been shown to be affected by anesthetics (for review, see Franks, 2008; Hemmings et al., 2005). First, almost all anesthetics including isoflurane and α-chloralose (Garrett and Gan, 1998) potentiate $GABA_A$ receptor-mediated responses. Second, the opening of potassium channels by anesthetics also seems important and two-pore-domain K^+ channels (2PK) are more or less activated by volatile anesthesia. No 2PK channels have been shown to be affected by clinically relevant intravenous anesthetics. Activation of either $GABA_A$ receptors or 2PK channels or both suppress neural excitability. Third, NMDA receptors are also a target for certain anesthetics. Most inhalation anesthetics, including isoflurane and nitrous oxide, inhibit NMDA receptors. This finding is intriguing because the activation of NMDA receptors seems to contribute significantly to hemodynamic responses (Gsell et al., 2006; Norup Nielsen and Lauritzen, 2001). The degree of these receptor modulations can be varied among anesthetic types, resulting in different neuronal excitabilities for different anesthetics. In our previous experiments, we found that a post-stimulus refractory period of the neural response was very short under isoflurane compared to α-chloralose (Fig. 3A of Masamoto et al., 2007). This suggests that high frequency stimuli induce less neural adaptation under isoflurane anesthesia than α-chloralose and that the maximal neural activity per unit time would also shifts to higher stimulus frequency under isoflurane compared to α-chloralose anesthesia.

Inhalation anesthetics enable the maintenance of a stable anesthetic plane for the long periods of time and also allow for the easy and relatively fast control of the depth of anesthesia (Lukasik and Gillies, 2003). Furthermore, animals under the inhalation anesthesia can recover within minutes after discontinuing inhalant administration, which makes it ideal for the repetition of survival studies in the same animals (Lukasik and Gillies, 2003). Instead of inhaled anesthetics, injectable anesthetics can also be used for survival experiments. Generally injectable, particularly intravenous, anesthetics affect somatosensory-evoked potentials less than inhaled anesthetics (Banoub et al., 2003). As a result, medetomidine was used for survival fMRI experiments (Weber et al., 2006). Since medetomidine has a reversal agent – antisedan – it can also assist the recovery from anesthesia. However, medetomidine changes the baseline physiological conditions (e.g. increases mean arterial blood pressure) (Weber et al., 2006), and consequently fMRI responses are likely to be affected, resulting in different responses from repetitive measurements in the same imaging sessions. In addition, it is typically used subcutaneously, although intravenous administration is also possible, and its effects will not be as quick as inhaled anesthetics. Other anesthetics may also be suitable for fMRI longitudinal experiments. Regardless, the choice of anesthetic and anesthesia depth will be likely influence the optimal stimulus frequency in the system being investigated. We have summarized the stimulus parameters for the maximal response induced by rat forepaw stimulation under different types of anesthesia in Table 1. As mentioned earlier, the optimal frequency under α-chloralose anesthesia was consistently observed at 1–3 Hz. Van Camp et al. reported that the optimal response frequency for BOLD responses shifted from 1 Hz with 0.3 ms pulse width to 8–10 Hz with 10 ms pulse width under α-chloralose anesthesia (Van Camp et al., 2006). This indicates that different stimulus pulse width may also influence in the evoked vascular responses. The stimulus amplitude and width were not manipulated in our present experiments, instead they were selected based on our previous findings (Masamoto et al., 2007). The stimulus amplitude (~1.5 mA current) was below the threshold of nociception where the stimulation evokes systemic arterial blood pressure changes, indicating painful stimulation. The stimulus pulse width (1.0 ms) was found to be the lower end of the range that evokes steady-state neural responses (Masamoto et al., 2007). A subtle difference in the location of stimulating needles (probes) on forepaw also could affect to our frequency-dependent responses because different type of sensory receptors and fibers could be stimulated between different animals. However, the same stimulus frequency-dependency observed between animals rules out the significant contribution of this factor to our results.

We observed a slight discrepancy between the CBF_{LDF} and CBF_{ASL} measurements; the CBF_{LDF} changes were higher than CBF_{ASL} (Figs. 2B and 5B). Potential sources for this discrepancy may be physiological and methodological differences between the two measurements. Two separate animal groups were used for the CBF_{LDF} and CBF_{ASL} studies. Although the physiological parameters measured in the baseline periods were not different between the two groups, the magnitude of functional responses may be different due to the limited number of animals studied in each group. Methodological differences between the two modalities may also be the major source of this discrepancy. Since the sensitivity volume of LDF is not precisely known, CBF_{LDF} and CBF_{ASL} signals were not obtained from identical brain regions. Technically, CBF measured by LDF reflects the changes in scattered light due to the movement of red blood cells (RBC) which produces a Doppler shift. Thus, LDF data are weighted to the changes in RBC flow or concentration (Stern, 1975). In contrast, ASL fMRI signals arise from spin-labeled plasma and RBC water, and thus likely represent total blood flow (Williams et al., 1992). Therefore, the mismatch of LDF and ASL responses in this study can be caused by the different signal source of two different modalities. It is possible that for large CBF changes (such as the ones observed for stimulus frequencies of 6 and

Table 1
Stimulus parameters for the maximal response by rat forepaw stimulation in literatures.

Anesthetic	Measurements	Range of frequency (Hz)	Pulse width (ms)	Pulse amplitude (mA)	Stimulus duration (s)	Optimal frequency (Hz)	Ref.
Isoflurane	FP/CBF_{LDF}/BOLD/CBF_{ASL}	1–24	1.0	1.5	30 (<10)	6–8 (8–12)	Present study
Enflurane	OIS/SEP	2–20	1.0	1	2	10	Sheth et al. (2003)
α-chloralose	CBF_{LDF}	1–5	0.3	1.5	40	3	Silva et al. (1999)
	BOLD/SEP	1.5–6	0.3	0.5	50	1.5	Brinker et al. (1999)
	BOLD	1.5–9	0.3	0.5	40	1.5–3	Gyngell et al. (1996)
	BOLD	1–8	0.3	2.0	30–45	3	Keilholz et al. (2004)
	BOLD	0.5–12	0.3	2	30	1.5	Sanganahalli et al. (2008)
	BOLD	1–10	0.3	2.0	4/32	3–5	Kida and Yamamoto (2008)
	BOLD/FP	1–15	0.3	1–1.2	30	1–3	Huttunen et al. (2008)
	BOLD/SEP	1–12	10	1.0	40	8–10	Van Camp et al. (2006)
Urethane	BOLD/FP	1–15	0.3	1–1.2	30	>11	Huttunen et al. (2008)
Medetomidine	BOLD	1–18	0.3	2	20	9	Zhao et al. (2008)

OIS: optical intrinsic signal.
SEP: somatosensory-evoked potentials.
Pubmed keyword: rat somatosensory forepaw stimulation frequency.

12 Hz), the changes in RBC and plasma flow may be dissociated. If RBC flux (velocity × volume) increases more than plasma flux, then the percentage change of LDF due to stimulation could be higher than that of ASL.

Our findings suggest that the stimulus frequency for a maximal signal change needs to be adjusted depending on stimulus duration due to neural adaptation (and also anesthesia when considering other reports in the literature). Under 1.3–1.5% isoflurane anesthesia, maximal neural and vascular signal changes induced by forepaw stimulation were obtained with a stimulus frequency of 6–8 Hz for a stimulus duration of 30 s, and 8–12 Hz for shorter stimulus durations (<10 s). The number of active pixels with stimulus time-dependent fMRI results was also dependent on the stimulus frequency. The number of active pixels was significantly decreased with increasing stimulus period for a stimulus frequency of 12 Hz, while it was relatively unaffected for lower stimulus frequencies (Fig. 4). This suggests that a stimulus frequency of 12 Hz is a good choice for event-related fMRI studies with short stimulus duration, while a frequency of 6–8 Hz would be optimal for block-design fMRI studies with longer stimulus duration (over 15 s) including ASL fMRI studies, which requires a long TR due to the spin-preparation time. To detect the maximal fMRI responses for a given experimental time, the combination of a short stimulation period and high stimulation frequency is probably the best choice since this would be reduce the inter-stimulus period and allow more averages. Further systematic studies are necessary by performing experiments with different stimulus durations and inter-stimulus periods. The GLM analysis performed and found that the number of activated pixels was not affected by stimulus frequency (Fig. 4). For this analysis, we obtained a gamma function for each frequency using average time courses, in which the neural adaptation is reflected. In a traditional GLM analysis, a hemodynamic response function (such as short stimulation) is convolved with experimental stimulus function assuming no neural adaptation. Maps of the GLM analysis with a *predicted* reference function will be similar to maps with a 30-s box-car function (see supplementary material for *t*-test maps with 30-s box-car reference. Thus, it is important to consider neural adaption in the GLM analysis). It should be noted that the depth of anesthesia could affect neural adaption and the hemodynamic response (Masamoto et al., 2009). Therefore, experiments with different depths of isoflurane anesthesia or stimulus durations longer than 30 s should recalibrate the experimental condition with the neural and hemodynamic responses. Similarly, the forepaw stimulation parameters that have been optimized for isoflurane-anesthetized rats may not be directly translatable to other species.

Acknowledgments

We thank Drs. Iwao Kanno and Takayuki Obata for valuable discussions on the vascular responses and Dr. Daniel Simons for discussion on neural adaption. This study was supported by the National Institutes of Health (EB003375, EB003324, and NS044589).

Appendix A. Supplementary data

Supplementary data associated with this article can be found, in the online version, at doi:10.1016/j.neuroimage.2010.03.064.

References

Alkire, M.T., Hudetz, A.G., Tononi, G., 2008. Consciousness and anesthesia. Science 322, 876–880.
Banoub, M., Tetzlaff, J.E., Schubert, A., 2003. Pharmacologic and physiologic influences affecting sensory evoked potentials: implications for perioperative monitoring. Anesthesiology 99, 716–737.
Barbier, E.L., Silva, A.C., Kim, H.J., Williams, D.S., Koretsky, A.P., 1999. Perfusion analysis using dynamic arterial spin labeling (DASL). Magn. Reson. Med. 41, 299–308.
Bock, C., Krep, H., Brinker, G., Hoehn-Berlage, M., 1998. Brainmapping of alpha-chloralose anesthetized rats with T2*-weighted imaging: distinction between the representation of the forepaw and hindpaw in the somatosensory cortex. NMR Biomed. 11, 115–119.
Brinker, G., Bock, C., Busch, E., Krep, H., Hossmann, K.A., Hoehn-Berlage, M., 1999. Simultaneous recording of evoked potentials and T2*-weighted MR images during somatosensory stimulation of rat. Magn. Reson. Med. 41, 469–473.
Carandini, M., Ferster, D., 1997. A tonic hyperpolarization underlying contrast adaptation in cat visual cortex. Science 276, 949–952.
Castro-Alamancos, M.A., 2004. Absence of rapid sensory adaptation in neocortex during information processing states. Neuron 41, 455–464.
Chung, S., Li, X., Nelson, S.B., 2002. Short-term depression at thalamocortical synapses contributes to rapid adaptation of cortical sensory responses in vivo. Neuron 34, 437–446.
Colonnese, M.T., Phillips, M.A., Constantine-Paton, M., Kaila, K., Jasanoff, A., 2008. Development of hemodynamic responses and functional connectivity in rat somatosensory cortex. Nat. Neurosci. 11, 72–79.
DeBruyn, E.J., Bonds, A.B., 1986. Contrast adaptation in cat visual cortex is not mediated by GABA. Brain Res. 383, 339–342.
Dijkhuizen, R.M., Ren, J., Mandeville, J.B., Wu, O., Ozdag, F.M., Moskowitz, M.A., Rosen, B. R., Finklestein, S.P., 2001. Functional magnetic resonance imaging of reorganization in rat brain after stroke. Proc. Natl. Acad. Sci. U. S. A. 98, 12766–12771.
Dijkhuizen, R.M., Singhal, A.B., Mandeville, J.B., Wu, O., Halpern, E.F., Finklestein, S.P., Rosen, B.R., Lo, E.H., 2003. Correlation between brain reorganization, ischemic damage, and neurologic status after transient focal cerebral ischemia in rats: a functional magnetic resonance imaging study. J. Neurosci. 23, 510–517.
Franks, N.P., 2008. General anaesthesia: from molecular targets to neuronal pathways of sleep and arousal. Nat. Rev. Neurosci. 9, 370–386.
Garrett, K.M., Gan, J., 1998. Enhancement of gamma-aminobutyric acidA receptor activity by alpha-chloralose. J. Pharmacol. Exp. Ther. 285, 680–686.
Gsell, W., Burke, M., Wiedermann, D., Bonvento, G., Silva, A.C., Dauphin, F., Buhrle, C., Hoehn, M., Schwindt, W., 2006. Differential effects of NMDA and AMPA glutamate receptors on functional magnetic resonance imaging signals and evoked neuronal activity during forepaw stimulation of the rat. J. Neurosci. 26, 8409–8416.
Gyngell, M.L., Bock, C., Schmitz, B., Hoehn-Berlage, M., Hossmann, K.A., 1996. Variation of functional MRI signal in response to frequency of somatosensory stimulation in alpha-chloralose anesthetized rats. Magn. Reson. Med. 36, 13–15.
Hemmings Jr., H.C., Akabas, M.H., Goldstein, P.A., Trudell, J.R., Orser, B.A., Harrison, N.L., 2005. Emerging molecular mechanisms of general anesthetic action. Trends Pharmacol. Sci. 26, 503–510.
Herscovitch, P., Raichle, M.E., 1985. What is the correct value for the brain–blood partition coefficient for water? J. Cereb. Blood Flow Metab. 5, 65–69.
Huttunen, J.K., Grohn, O., Penttonen, M., 2008. Coupling between simultaneously recorded BOLD response and neuronal activity in the rat somatosensory cortex. Neuroimage 39, 775–785.
Keilholz, S.D., Silva, A.C., Raman, M., Merkle, H., Koretsky, A.P., 2004. Functional MRI of the rodent somatosensory pathway using multislice echo planar imaging. Magn. Reson. Med. 52, 89–99.
Khatri, V., Hartings, J.A., Simons, D.J., 2004. Adaptation in thalamic barreloid and cortical barrel neurons to periodic whisker deflections varying in frequency and velocity. J. Neurophysiol. 92, 3244–3254.
Kida, I., Hyder, F., Behar, K.L., 2001. Inhibition of voltage-dependent sodium channels suppresses the functional magnetic resonance imaging response to forepaw somatosensory activation in the rodent. J. Cereb. Blood Flow Metab. 21, 585–591.
Kida, I., Yamamoto, T., 2008. Stimulus frequency dependence of blood oxygenation level-dependent functional magnetic resonance imaging signals in the somatosensory cortex of rats. Neurosci. Res. 62, 25–31.
Kim, T., Hendrich, K.S., Masamoto, K., Kim, S.G., 2007. Arterial versus total blood volume changes during neural activity-induced cerebral blood flow change: implication for BOLD fMRI. J. Cereb. Blood Flow Metab. 27, 1235–1247.
Kim, T., Kim, S.G., 2002. Dynamics of arterial labeled spins investigated by using 2-coil DASL. Proc 10th Annual Meeting, ISMRM, Hawaii, U.S.A, p. 1061.
Kim, T., Kim, S.G., 2005. Quantification of cerebral arterial blood volume and cerebral blood flow using MRI with modulation of tissue and vessel (MOTIVE) signals. Magn. Reson. Med. 54, 333–342.
Kohn, A., 2007. Visual adaptation: physiology, mechanisms, and functional benefits. J. Neurophysiol. 97, 3155–3164.
Krukowski, A.E., Miller, K.D., 2001. Thalamocortical NMDA conductances and intracortical inhibition can explain cortical temporal tuning. Nat. Neurosci. 4, 424–430.
Lee, S.P., Silva, A.C., Ugurbil, K., Kim, S.G., 1999. Diffusion-weighted spin-echo fMRI at 9.4 T: microvascular/tissue contribution to BOLD signal changes. Magn. Reson. Med. 42, 919–928.
Lukasik, V.M., Gillies, R.J., 2003. Animal anaesthesia for in vivo magnetic resonance. NMR Biomed. 16, 459–467.
Mandeville, J.B., Marota, J.J., Kosofsky, B.E., Keltner, J.R., Weissleder, R., Rosen, B.R., Weisskoff, R.M., 1998. Dynamic functional imaging of relative cerebral blood volume during rat forepaw stimulation. Magn. Reson. Med. 39, 615–624.
Masamoto, K., Fukuda, M., Vazquez, A., Kim, S.G., 2009. Dose-dependent effect of isoflurane on neurovascular coupling in rat cerebral cortex. Eur. J. Neurosci. 30, 242–250.
Masamoto, K., Kim, T., Fukuda, M., Wang, P., Kim, S.G., 2007. Relationship between neural, vascular, and BOLD signals in isoflurane-anesthetized rat somatosensory cortex. Cereb. Cortex 17, 942–950.
McLean, J., Palmer, L.A., 1996. Contrast adaptation and excitatory amino acid receptors in cat striate cortex. Vis. Neurosci. 13, 1069–1087.

Norup Nielsen, A., Lauritzen, M., 2001. Coupling and uncoupling of activity-dependent increases of neuronal activity and blood flow in rat somatosensory cortex. J. Physiol. 533, 773–785.
Paxinos, G., Watson, C., 1986. The Rat Brain in Stereotaxic Coordinates. Academic Press, San Diego.
Petersen, C.C., 2002. Short-term dynamics of synaptic transmission within the excitatory neuronal network of rat layer 4 barrel cortex. J. Neurophysiol. 87, 2904–2914.
Sanganahalli, B.G., Herman, P., Hyder, F., 2008. Frequency-dependent tactile responses in rat brain measured by functional MRI. NMR Biomed. 21, 410–416.
Schmitz, B., Bock, C., Hoehn-Berlage, M., Kerskens, C.M., Bottiger, B.W., Hossmann, K.A., 1998. Recovery of the rodent brain after cardiac arrest: a functional MRI study. Magn. Reson. Med. 39, 783–788.
Sheth, S., Nemoto, M., Guiou, M., Walker, M., Pouratian, N., Toga, A.W., 2003. Evaluation of coupling between optical intrinsic signals and neuronal activity in rat somatosensory cortex. Neuroimage 19, 884–894.
Sheth, S.A., Nemoto, M., Guiou, M., Walker, M., Pouratian, N., Toga, A.W., 2004. Linear and nonlinear relationships between neuronal activity, oxygen metabolism, and hemodynamic responses. Neuron 42, 347–355.
Silva, A.C., Kim, S.G., 1999. Pseudo-continuous arterial spin labeling technique for measuring CBF dynamics with high temporal resolution. Magn. Reson. Med. 42, 425–429.
Silva, A.C., Lee, S.P., Yang, G., Iadecola, C., Kim, S.G., 1999. Simultaneous blood oxygenation level-dependent and cerebral blood flow functional magnetic resonance imaging during forepaw stimulation in the rat. J. Cereb. Blood Flow Metab. 19, 871–879.
Silverman, J., Muir III, W.W., 1993. A review of laboratory animal anesthesia with chloral hydrate and chloralose. Lab. Anim. Sci. 43, 210–216.
Stern, M.D., 1975. In vivo evaluation of microcirculation by coherent light scattering. Nature 254, 56–58.
Ureshi, M., Matsuura, T., Kanno, I., 2004. Stimulus frequency dependence of the linear relationship between local cerebral blood flow and field potential evoked by activation of rat somatosensory cortex. Neurosci. Res. 48, 147–153.
Van Camp, N., Verhoye, M., Van der Linden, A., 2006. Stimulation of the rat somatosensory cortex at different frequencies and pulse widths. NMR Biomed. 19, 10–17.
Vidyasagar, T.R., 1990. Pattern adaptation in cat visual cortex is a co-operative phenomenon. Neuroscience 36, 175–179.
Weber, R., Ramos-Cabrer, P., Wiedermann, D., van Camp, N., Hoehn, M., 2006. A fully noninvasive and robust experimental protocol for longitudinal fMRI studies in the rat. Neuroimage 29, 1303–1310.
Williams, D.S., Detre, J.A., Leigh, J.S., Koretsky, A.P., 1992. Magnetic resonance imaging of perfusion using spin inversion of arterial water. Proc. Natl. Acad. Sci. U. S. A. 89, 212–216.
Zhao, F., Zhao, T., Zhou, L., Wu, Q., Hu, X., 2008. BOLD study of stimulation-induced neural activity and resting-state connectivity in medetomidine-sedated rat. Neuroimage 39, 248–260.